

Article

A Novel Slickwater System with Strong-Polarity Fibers for High-Efficiency Proppant Flowback Mitigation

Yang Xu ^{1,2,*}, Ping Chen ^{1,2}, Kun Wang ^{1,2}, Suoliang Wang ^{1,2}, Qingcong Meng ^{1,2}, Mingqi Li ^{1,2}, Yingxian Ma ^{3,4} and Jie Zeng ^{3,4,*}

¹ Research Institute of Drilling & Production Engineering, CNPC Chuanqing Drilling Engineering Company Limited, Xi'an 710018, China; chen_ping@cnpcc.com.cn (P.C.); wk_gcy@cnpcc.com.cn (K.W.); wangsl_gcy@cnpcc.com.cn (S.W.); mqc_gcy@cnpcc.com.cn (Q.M.); czzcylmq@cnpcc.com.cn (M.L.)

² National Engineering Laboratory for Exploration and Development of Low-Permeability Oil & Gas Fields, Xi'an 710018, China

³ Petroleum Engineering School, Southwest Petroleum University, Chengdu 610500, China; mayingxian@swpu.edu.cn

⁴ National Key Laboratory of Oil and Gas Reservoir Geology and Exploitation, Southwest Petroleum University, Chengdu 610500, China

* Correspondence: xy_gcy@cnpcc.com.cn (Y.X.); jie.zeng@swpu.edu.cn (J.Z.)

Abstract: To avoid or mitigate proppant flowback after a massive hydraulic fracturing of tight formations and to reduce its impairment to well productivity, this study developed a new type of fiber material with strong polarity based on polyester fiber. This fiber material is modified by introducing a strong-polar functional monomer into the molecular structure and adopting the means of surface grafting. On the basis of this fiber material, a fiber slip-water system with excellent dispersion performance can be established to prevent proppant backflow. Laboratory experiments were performed to analyze the specific function of the fibers with strong polarity and its working mechanisms. The results indicate that strong-polarity fibers have excellent dispersion performance. The fibers and resistance-reducing agents form an interwoven structure that can carry proppants, resulting in the enhancement of the sand-carrying capacity of the fracturing fluid system and the overall strength of the sand bank. In terms of the sand-carrying capacity and mitigation of proppant flowback, strong-polar fibers have significantly improved compared to unmodified fibers. In a 5 mm simulated crack, strong-polar fibers can increase the static settling time of 70/140 mesh quartz sand proppant by 26.5%. Meanwhile, the placement height of the sand embankment increased by 23.4% after the settlement of the proppant. In proppant transport experiments, strong-polar fibers with a mass fraction of 0.4% can increase the transport distance of proppants by more than 50%. Within the closed stress range of 2–10 MPa, the concentration of 0.5% strong-polar fibers increases the critical sand flow rate of the proppant by more than twice. The strong-polarity fiber system introduced in this study can be used to develop a fiber slickwater fracturing fluid system suitable for the massive hydraulic fracturing of tight reservoirs and has broad application prospects in the field of proppant flowback mitigation in tight reservoirs.

Keywords: strong-polarity fiber; fiber fracturing fluid; proppant carrying capacity; proppant flowback mitigation



Citation: Xu, Y.; Chen, P.; Wang, K.; Wang, S.; Meng, Q.; Li, M.; Ma, Y.; Zeng, J. A Novel Slickwater System with Strong-Polarity Fibers for High-Efficiency Proppant Flowback Mitigation. *Processes* **2024**, *12*, 724. <https://doi.org/10.3390/pr12040724>

Academic Editor: Adina Musuc

Received: 27 February 2024

Revised: 25 March 2024

Accepted: 29 March 2024

Published: 3 April 2024



Copyright: © 2024 by the authors. Licensee MDPI, Basel, Switzerland. This article is an open access article distributed under the terms and conditions of the Creative Commons Attribution (CC BY) license (<https://creativecommons.org/licenses/by/4.0/>).

1. Introduction

Horizontal-well massive hydraulic fracturing is currently the most popular technology for tight oil and gas extraction [1,2]. This technology enables the creation of complex fracture networks within the reservoir, enhancing the fracture–reservoir contact area and achieving long-term stable production of oil and gas wells [3]. In the process of reservoir fracturing, a large amount of fracturing fluid and proppant are injected into the reservoir, forming a complex artificial fracture network to improve the permeability of the reservoir.

After the completion of fracturing construction, a large amount of fluid injected into oil and gas wells needs to be flowed back before they can be put into production. In the process of drainage and production, proppant particles will destabilize and move in fractures and gradually migrate to the wellbore, resulting in sand production in oil and gas wells [4]. One field example in the Changqing Oilfield, the largest oil and gas field in China, indicates that the produced proppant volume for a single well varies from 9 m³ to 70 m³, while the average value is 23.3 m³. Proppant back production not only causes damage in the proppant bank [5] but also reduces the proppant supporting efficiency, which generates certain impairment on the long-term conductivity and productivity [6,7]. Apart from that, the back-produced proppants within the wellbore are deposited at the well bottom and also plug the production layer, which increases the difficulty for dealing with the wellbore [8]. When the fracturing fluid flowback rate or the production rate is high, proppants may flow out from the wellhead and cause damage to the choke and pipelines [9], leading to potential safety issues.

The generation of proppant backflow is closely related to the fluid flow in the fracture. The fluid flow in the reservoir after fracturing mainly covers the matrix flow, natural micro-fracture flow, and artificial fracture flow [10]. The fracturing flowback fluid and oil and gas seepage in fractures and porous media are extremely complex [11]. The process of proppant movement in fractures is a fluid–solid coupling physical process. The movement state of proppant particles depends on the physical properties of particles and fluids, the flow field distribution in fractures, the pressure field distribution, and the distribution of solid particles [12]. Affected by factors such as fluid velocity and viscosity [13,14], the proppant moves in the fracture and flows back into the wellbore with the flow of oil, gas, and fracturing fluid [15]. This backflow may occur after hydraulic fracturing or during the pressure redistribution process during well switching [16].

Using fibers can effectively improve the proppant settling profile [17,18], and eventually mitigate or avoid proppant back production [19]. Hu et al. [20] added polypropylene fiber to the fracturing fluid to resist proppant backflow. The complex three-dimensional network structure formed by fibers and ceramsite was observed with microstructure. A single fiber can intercept and fix 6~8 20/40 mesh ceramsite along the length direction, which effectively improves the overall compressive strength of proppant particles. Chen et al. found that the fiber can significantly improve the strength of the proppant filling layer through experimental research, and the addition of the fiber makes the proppant filling layer better resist the erosion of the backflow fluid. The critical velocity with fiber is 2.25 times higher than that without fiber. In recent years, the fiber-based proppant flowback mitigation technology has been applied to many tight gas and oil horizontal wells. However, the surface of classical fibers lacks active functional groups, and these fibers have poor dispersibility in fracturing fluids [21] and poor suitability for proppants. This fiber–proppant mixture can hardly form a stable structure so that proppants can easily flow out. In addition, due to the relatively large density difference between proppants and fibers and the use of low-viscosity slickwater in tight formations [22], the gravity differentiation of proppants and fibers frequently occurs along the fracture height direction, impairing the application efficiency.

To address the above-mentioned challenges, this study developed a new type of fiber material with strong polarity. Through the introduction of highly polar functional monomers and surface modification, the coupling among fibers, drag reducers, and proppant particles is greatly enhanced, improving the stability of the fiber–proppant interwoven structure. The new strong-polarity fiber system can be used to develop a fiber slickwater fracturing fluid system that has good dispersibility and can mitigate or avoid proppant back production. This technology will strongly support the efficient development of tight oil and gas reservoirs and solve the problem of proppant flowback after massive hydraulic fracturing in tight reservoirs.

2. Basic Mechanisms

2.1. Proppant Flowback Mechanisms

After a fracturing treatment, the well starts to produce fracturing fluids and hydrocarbon. When the fluid flow rate approaches a critical value, the injected proppant particles are influenced by the drag force of the fluid. The proppant particles gradually transition from a steady state to an unstable state, resulting in the phenomenon of “fluidization” [23]. Thus, the fluid carries proppants and flows into the wellbore and finally flows out from the wellbore [24]. This process refers to proppant backflow or back production. With the continuous backflow of proppants, the stability of the proppant pack is further destroyed, leading to more serious proppant back production [25].

Figure 1 shows the specific force analysis of a single proppant particle during the later stage of oil and gas well backflow and the production process. During the processes of fracturing fluid flowback and oil and gas production, the force that acts on proppants in the horizontal direction can be divided into two types: backflow driving force F and backflow resistance f . The driving force F mainly includes the drag force acting on the proppant particles as the fluid flows P_{drag} and the equivalent capillary force of the residual fluid within the fracture acting on the proppant σ_c [26]. The drag force exerted by the fluid on the particles can fluidize the proppants and is the main force causing the proppant flowback. The magnitude of equivalent capillary force is equal to that of the capillary force but is in an opposite direction compared with the capillary force. As for the backflow resistance f , it includes the force from the fracture wall acting on the proppant pack f_c and the interaction forces between proppant particles f_p . The force from the fracture wall mainly refers to the closure pressure perpendicular to the wall. It can crush the proppants or induce an axial extrusion force to extrude the proppants. The interaction forces involve cohesion and friction between particles [27]. The interaction forces make proppants attract each other and limit their movement [28].

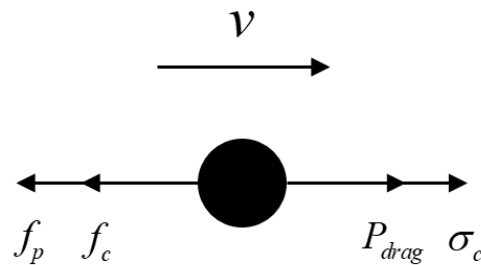


Figure 1. Force diagram of a single proppant.

Based on the force distribution of the proppant particles, a physical model for the force distribution of a single proppant particle in a crack is proposed, as shown in Equation (1). The critical condition under which the proppant will flow back is that the backflow driving force is larger or equal to the backflow resistance. When the driving force is smaller than the backflow resistance, the proppant pack remains structurally stable, and the proppant flowback will not happen. In contrast, when the driving force is larger than the backflow resistance, proppant particles are controlled by the fluid drag force, promoting proppant migration with the fluid flow. The structure of the proppant pack becomes unstable, which further causes more proppants to flow back into the wellbore and induces sand production from the wellbore.

$$\begin{cases} F = P_{drag} + \sigma_c \\ f = f_c + f_p \end{cases} \quad (1)$$

where P_{drag} is the fluid drag force (MPa), σ_c is the equivalent capillary force (MPa), and f_c is the force component of the closure stress acting on the proppants in the flow velocity direction (MPa). Figure 1 shows the corresponding force diagram.

2.2. Mechanism of Proppant Backflow Control Using Fibers

The fiber-containing fracturing technology is currently the most widely-used technology to prevent proppant flowback. This technology involves adding a fibrous material with certain flexibility to the sand-carrying fluid and pumping the mixture into the formation. The proppant sand bank serves as the base phase, while the fibers are the reinforcing phase, forming a composite proppant pack structure within artificial fractures [29,30]. The fiber materials make the proppant pack stable, and it is chemically stable. Thus, the wells can directly start the fracturing fluid flowback process without a shut-in. In this way, the critical fluid flow rate in the hydraulic fracture can be significantly increased. This technology has advantages, such as broad applicability, low cost, and simplicity of use. Consequently, in oil and gas wells with a serious proppant-backflow phenomenon, the fiber-containing fracturing technology has become a common choice to solve this issue.

The mechanism of the reinforcement of the proppant pack by adding the fibrous materials can be explained by the composite material theory [31]. The mixing of fibers into the proppant pack plays a role similar to the addition of a steel skeleton to concrete, as shown in Figure 2. The fibers are intertwined with each other and distributed in the sand body to form a 3D network structure [32]. Meanwhile, each fiber is in contact with several proppant particles [33] and interacts with each other through contact pressure and friction, thereby enhancing the cohesion of the proppants and improving the stability of the proppant pack. During the fracturing fluid backflow process, gel-breaking fracturing fluid and hydrocarbons flow freely through the pore structure of the fiber–proppant composite sand bank. The fluid flow has a scouring effect on proppants, which causes the proppant particles to undergo shear deformation and form a sand arch, and the shear deformation of the sand arch induces fiber deformation [34]. The stress transmission of the fiber makes the axial force of the fiber decompose into two parts: the tangential component and the normal component, which can resist the shear deformation of the sand arch and stabilize the proppant pack, thereby enhancing the anti-scouring ability of the proppants and the critical flow rate and achieving the goal of proppant backflow mitigation or prevention.

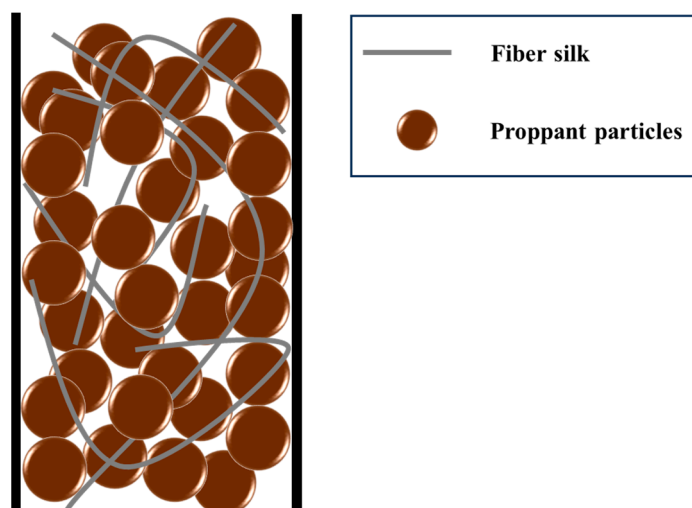


Figure 2. Schematic diagram of the mechanism of proppant flowback prevention using fibers.

3. Experimental Research

First, by introducing strong-polar functional monomers and surface modification, strong-polarity fiber materials were prepared in the laboratory. After the preparation of fibers, the functional characteristics and mechanism of action of the fibers were studied through laboratory experiments. The experimental process is shown in the Figure 3. The degree of performance improvement relative to unmodified fibers was evaluated by testing the microstructure characteristics, dispersion performance, dynamic and static sand carrying performance, and proppant flowback mitigation of strongly polar fiber systems.

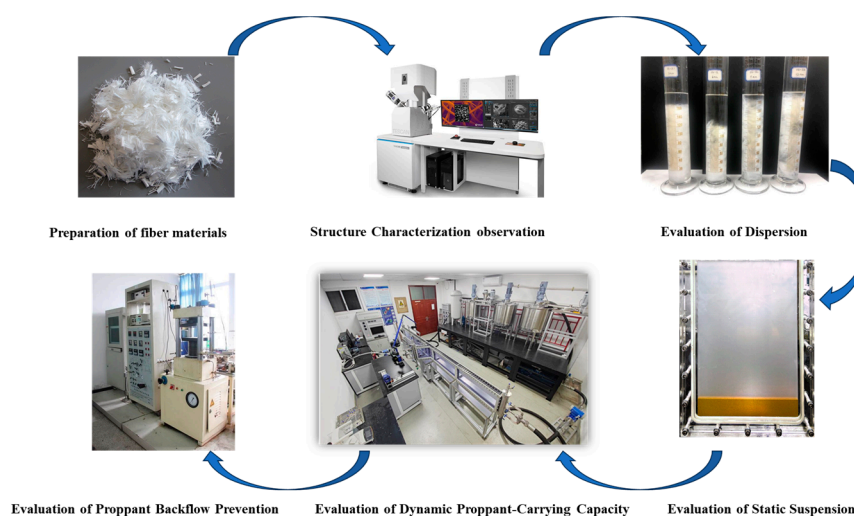


Figure 3. Experimental process for evaluating the performance of fiber systems.

3.1. Materials and Apparatus

The experimental materials mainly include phthalic acid (PTA), purchased from Shanghai Huichao New Materials Co., Ltd. (Shanghai, China); N-acryloyl glycinamide (NAGA), purchased from Guangdong Wengjiang Chemical Reagent Co., Ltd. (Shanghai, China); white oil, purchased from Shandong Xinsheng Chemical Co., Ltd. (Weifang, China); ethylene glycol (EG), dichloromethane (DCM), and palmitic acid monoglyceride (PAG) purchased from Chengdu Cologne Chemical Reagent Factory (Chengdu, China); and polyester fiber, purchased from Shandong Chenyu Engineering Materials Co., Ltd. (Jinan, China). The drag-reducing agent 0933-S5X was purchased from Chengdu Laoenpusi Technology Co., Ltd. (Chengdu, China). The 40/70 mesh quartz sand and 70/140 mesh quartz sand proppant with compressive strength of 70 MPa were purchased from Sichuan Chuanqing Underground Service Co., Ltd. (Chengdu, China). The purified ultrapure water was used to configure the solution.

The experimental instruments mainly included the following: high temperature esterification polycondensation esterification reactor produced by Weihai Huanyu Chemical Machinery Co., Ltd. (Weihai, China); zNN-D6 six-speed rotary viscometer produced by Ken Instrument (Shanghai) Co., Ltd. (Shanghai, China); Quanta 450 environmental scanning electron microscope produced by FEI, Hillsborough, Oregon, USA; rCT basic magnetic stirrer produced by IKA, Staufen, Germany; and electronic balance produced by Sartorius Scientific Instrument Co., Ltd. (Goettingen, Germany). Nanjing Lvding Machinery Equipment Co., Ltd. (Nanjing, China) produced hot air circulation oven. Other test instruments included fracture conductivity test system, proppant plate conveying device, and visual proppant settling device, all of which were laboratory self-assembled instruments.

3.2. Synthesis Process of Strong-Polarity Fibers

3.2.1. Principle of Synthesis Design

Polyester fibers are the raw materials of the strong-polarity fibers. In the polyester fiber polycondensation process, the method of controllable free radical polymerization is used to introduce the strong-polarity functional monomer (N-acryloyl glycinamide) into the molecular chain in a controllable manner, making the fiber-based polymer have uniform molecular weight and a regular structure. The fibers are made by melting and spinning the polymers. The surface grafting modification of the fiber was further carried out. Figure 4 shows the schematic diagram of the fiber surface grafting treatment. With the help of long-chain strong-polar surface modifier (Palmitic acid monoglyceride), specific strong-polar long-chain groups were grafted on the fiber surface to further enhance the hydrophilicity of the modified fiber while balancing the density of the material to

synthesize surface-modified strong-polar fiber materials, thereby solving the problem of poor compatibility between conventional fibers and proppants and liquid systems.

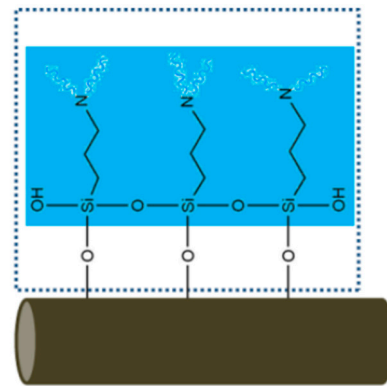


Figure 4. Schematic of the fiber surface grafting treatment. (The blue box contains strong polar long-chain functional groups grafted onto the fiber surface.).

The surface properties of the fiber materials were changed by the two-step treatment so that the fiber surface had better hydrophilicity, which could help improve fiber's wetting and dispersion properties in the fracturing fluid and also enhance the coupling with the hydrophilic proppant particles. Due to the change in surface properties, the fibers that are clumped together are more easily dispersed. Apart from that, the density of strong-polarity fibers can reach 1300 kg/m^3 , which is denser than that of conventional fiber materials, reducing the density difference between fibers and proppants and mitigating the fiber escape phenomenon. As a result, in the fiber-containing fracturing field applications, these fibers can help to form a more stable fiber–proppant composite structure.

3.2.2. Strong-Polarity Fiber Preparation Process

The schematic diagram of the preparation process of the strong-polarity fiber is shown in Figure 5. The synthesis process included the following five steps.

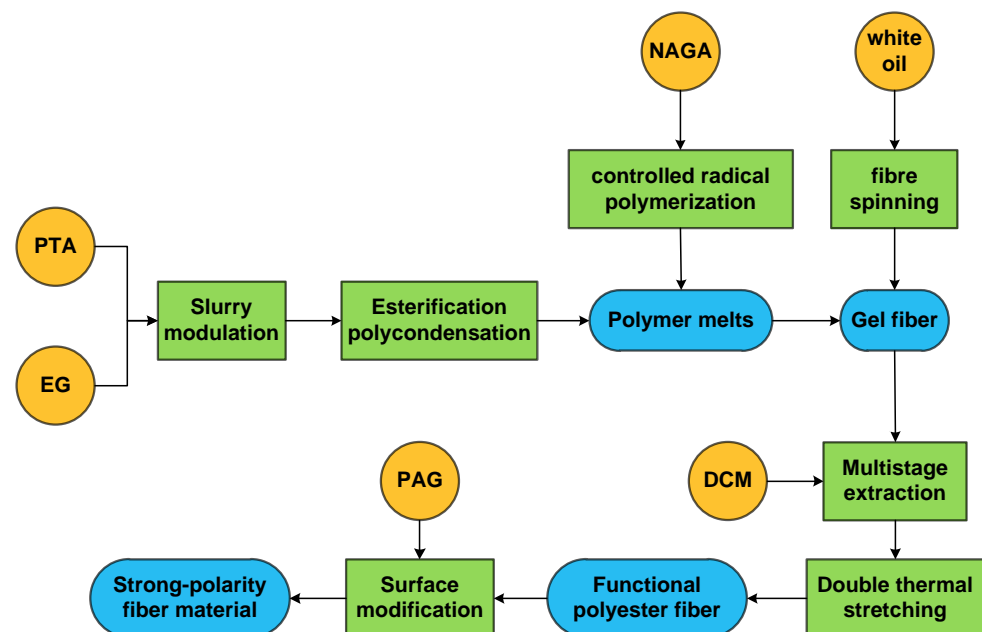


Figure 5. Flow chart of strong-polarity fiber preparation.

Step 1: polymer polymerization. The phthalic acid was sent into a U-shaped esterification kettle for esterification reaction under heating conditions of $240\text{--}290 \text{ }^\circ\text{C}$. By controlling

the amount of ethylene glycol and changing the reaction conditions, the esterification rate of the product was improved. By employing the controllable radical polymerization method, the N-acryloyl glycinamide was introduced into the molecular chain in a controllable manner, which made the molecular structure of the polymer more regular.

Step 2: spinning. The organic solvent wet gel spinning process was used to add the functional polyester fibers to the white oil. The polymer was swelled and dissolved in a twin-screw extruder and then extruded from the spinneret and quenched into a coagulation bath to form gel fibers. Methylene chloride was used as an extractant for multi-stage extraction. Dry fibers were prepared by extraction and drying. Then, the functional polyester fiber materials with diameters ranging from 7 μm to 20 μm and lengths ranging from 3 mm to 20 mm were obtained by superheating stretching. These materials have a large length-to-diameter ratio.

Step 3: surface modification. The palmitic acid monoglyceride was transferred into a three-neck flask. The flask was heated and the solution was stirred quickly to warm up to 40 °C to 60 °C. The functional polyester fibers were added to the three-neck flask. Then, the solution was fully stirred for 60 min to 80 min under a constant temperature condition. The above-mentioned constant temperature was set in the range of 40 °C to 60 °C.

Step 4: suction filtration. After surface modification, the functional polyester fibers were moved to the filter paper and cooled to room temperature. Then, suction filtration was performed.

Step 5: drying. The filtered fibers were placed in an oven at 60 °C to 80 °C for drying, and the drying time was between 16 h to 24 h. After that, the fibers preventing proppant backflow were obtained.

3.3. Experimental Method

3.3.1. Evaluation of Fiber Dispersion Properties

Unmodified fibers and strong-polarity fibers with different length-to-diameter ratios satisfying 0.5% mass fraction were added to 200 mL water and 200 mL slickwater with 0.1% mass fraction respectively. The fibers were stirred and dispersed evenly by a magnetic stirrer at a speed of 1000 r/min for 2 min. Then, the fiber suspension was quickly poured into a 250-mL graduated cylinder. After 2 h of settling, the dispersion state of the fibers in the solution was analyzed. The dispersity calculation equation was used to evaluate the dispersion properties of the fibers [35], see Equation (2).

$$y = \frac{h_0 - h_1}{h_0} \quad (2)$$

where h_0 is the height at which the fibers begin to precipitate in the fiber suspension (mm), h_1 is the height of the upper layer of water in the fiber suspension (mm), and y is the dispersity (%).

3.3.2. Evaluation of Proppant-Suspension Capacity of Fibers under Static Conditions

Static sand carrying performance test reference 'SY/T 5185-2016' [36] for testing. The unmodified fibers and 06-Q3-12-mm fibers with the best dispersion performance were added to 320 mL of ultrapure water. The mass fraction values of unmodified fibers and 06-Q3-12mm fibers were 0.1%, 0.3%, and 0.5%. The fibers were stirred and dispersed by a magnetic stirrer for 2 min.

After the fibers were evenly dispersed, 70/140 mesh quartz-sand proppants with a proppant concentration of 10% were added and stirred evenly. Then, drag-reducing agents with a mass fraction of 0.1% were further added. The mixtures with certain mass concentration values were prepared and stirred for 5 min to achieve uniform dispersion.

After the solution preparation was completed, the fiber-sand mixture was quickly transferred to the proppant settling visualization device (300 mm \times 200 mm \times 5 mm) to simulate the static settling of proppant particles within a 5 mm wide fracture in a tight

formation, analyze the settling state and placement efficiency, and calculate the static settling velocity and height of the proppant pack.

3.3.3. Evaluation of Proppant-Carrying Capacity

The strong-polar fiber with a mass fraction of 0.4%, the 40/70 mesh quartz sand proppant with a sand ratio of 10%, the resistance reducing agent with a mass fraction of 0.1%, and the rest of the water were added to the stirred tank to configure the fiber slickwater proppant-carrying fluid and configuration without fiber slickwater proppant-carrying fluid for comparison.

After preparation of the proppant carrying fluid, a certain amount of water was pumped into the 6 mm wide fracture to circulate the water and achieve a stable condition. Then, the uniformly mixed fluid containing fibers, drag reducer, proppants, and water was pumped into the flat fracture (300 cm × 60 cm × 6 mm) with an 18 L/min pumping rate.

When the proppant particles flowed through the observation area, the dynamic data in the experimental process were recorded through the high-definition video acquisition system. The transport and settlement states of the particles were observed through image analysis in a later stage.

3.3.4. Evaluation of Proppant Back Flow Prevention Performance

The method of measuring the critical flow rate was used to investigate the stability of the proppant pack [33]. The standard API conductivity tester was used, and the wall of the conductivity tester was made of CD-4MCu duplex stainless steel. In the proppant flowback control experiment, 40/70 mesh and 70/140 mesh proppants were used. Slickwater fracturing fluid with a mass fraction of 0.01% and 3 mPa·s viscosity was used to simulate the gel breaking and flowback stage of fracturing fluid. Specifically, the process of determining the critical flow rate of the proppant pack was as follows.

Step 1: After mixing the fiber materials and proppants uniformly with different concentrations, the mixture was placed between the two plates in the conductivity testing chamber with a placement concentration of 5 kg/m² to create a 2.5 mm wide artificial fracture.

Step 2: The loading on the plate was slowly added until the pressure reached the designed closure pressure. The slickwater was used to flush the artificial fracture. The displaced fluid amount gradually increased.

Step 3: Under different pressure conditions, slickwater flows in the proppant filling layer. When the flow rate reaches a certain speed, it causes the migration of proppant particles, and the proppant particles begin to flow out from the outlet of the diversion chamber. The sand production at the outlet of the conductivity testing chamber was observed, and the corresponding fluid flow rate at that time, which was the critical sand flow rate, was recorded.

3.3.5. Environmental Scanning Electron Microscope Test

Step 1: The drag reducer satisfying 0.1% mass fraction was added to 100 mL of ultrapure water. It was stirred and dispersed by the magnetic stirrer for 5 min, and the low-viscosity slickwater was configured. Then, 70/140 mesh quartz-sand proppants with a 20% concentration were further added to the slickwater. The fiber-free slickwater mixed sand liquid was obtained after being stirred and mixed uniformly.

Step 2: The strong-polarity fibers satisfying 0.5% mass fraction were added to 50 mL of proppant–slickwater mixture. Then, it was stirred for 5 min. Consequently, the low viscosity fiber–slickwater mixed sand liquid was obtained.

Step 3: A small amount of fiber-free slickwater mixed sand liquid and fiber-free slickwater mixed sand liquid were collected as samples for scan. The microscopic morphology of the mixed system of fibers, drag reducer, and proppants was observed and analyzed through environmental scanning electron microscope (ESEM).

4. Experimental Results and Discussion

4.1. Structure Characterization

The scanning electron microscope results of the fiber-free slickwater mixed sand liquid with a mass concentration of 0.1% are shown in Figure 6a. Without fibers, the molecular chain of the polymer of the drag reducer swells and stretches to form a network structure, which is wrapped and covered on the surface of the quartz sand particles, generating a certain fixing and connecting effect on the proppant. However, due to the weak network structure formed by the low-concentration drag reducer, the above effect is also weak. The scanning electron microscope results of the fiber–slickwater mixed sand liquid with the same concentration are shown in Figure 6b. When the strong-polarity fibers are added, the fibers are dispersed into filaments and interspersed in the proppant particles, and the drag reducer molecules encapsulate the proppant. The fiber is used as a rigid support body. Combined with the drag reducer, the mixture forms a network structure to wrap and carry proppants, and the coupling effect of fibers and proppants greatly enhances the overall structural strength of the proppant pack. The bonding of the fibers and the drag reducer forms a three-dimensional network structure with high strength, which greatly enhances the overall structural strength of the proppant bank, helps resist the external interference from the fluid, fixes the proppants network in their original position, and consequently maintains the stability of the sand body and prevents the backflow of the proppants.

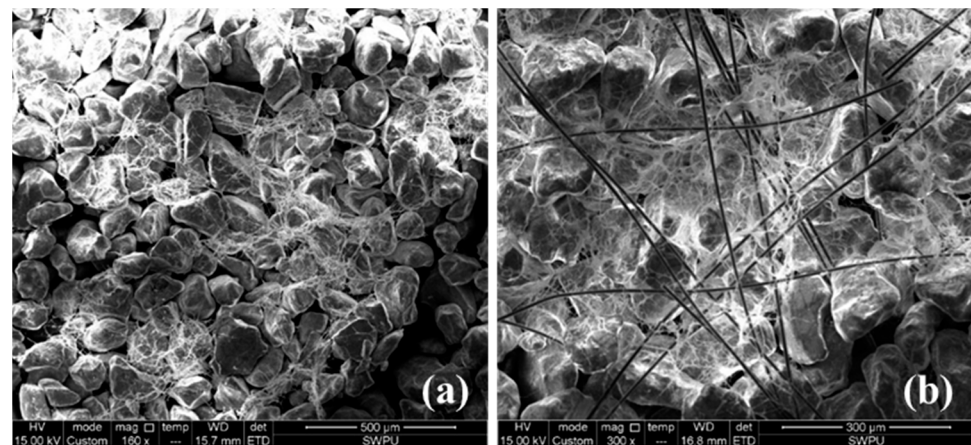


Figure 6. Scanning electron microscope photos of mixed sand slickwater system with and without strong-polarity fiber. (a) Fiber-free slickwater mixed sand liquid. (b) fiber–slickwater mixed sand liquid.

4.2. Evaluation of Fiber Dispersion Properties

The dispersion performance of the fiber materials affects the fracturing fluid preparation time in the field and also determines its effect on the proppant particles in the liquid system. Therefore, fiber dispersion experiments were carried out in clear water and slickwater fracturing fluids. The dispersion properties of different fibers in clear water and slickwater fracturing fluids were studied. Figure 7 shows the comparison of the dispersion behavior of unmodified fibers and strong-polarity fibers in clean water and slickwater with 0.1% mass fraction. Table 1 shows the dispersion performance of different fibers in clean water and slickwater. Taking the dispersion degree as the evaluation criterion, the more thorough the fiber dispersion is, the better the dispersion effect of the fiber in the solution would be.

Table 1. Evaluation results of dispersion properties of different fibers in clean water and slickwater.

Fibers	Solution	Dispersion Time of Fibers /s	Height of the Fibers Layer h_0 /cm	Height of the Water Layer h_1 /cm	Dispersivity/%
Unmodified fiber	Ultra-pure water	30	18.1	10.4	42.54
Strong-polarity fiber	Ultra-pure water	<10	17.7	0	100.00
Unmodified fiber	Slickwater	30	18.1	6.2	65.75
Strong-polarity fiber	Slickwater	<10	17.7	0	100.00

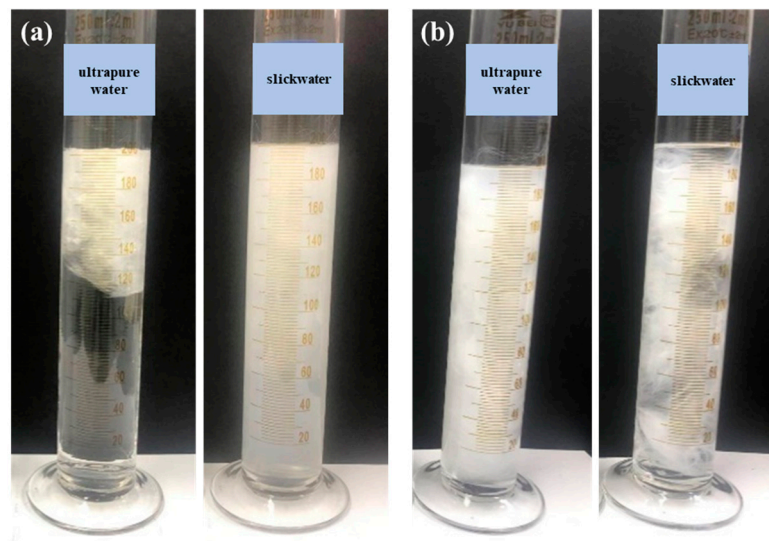


Figure 7. Comparison of the dispersion of different fibers in ultra-pure water and slickwater. (a) Unmodified fiber. (b) strong polar fiber.

The dispersion of unmodified fibers in ultra-pure water and slickwater is shown in Figure 7a. The dispersion time of unmodified fiber is about 30 s. The unmodified fibers were distributed by filament in the solution. Due to the small fiber density, most of the fibers floated to the upper part of the clean water-based solution after 2 h, and a large section of clear water stratification appeared in the lower part of the system; the fiber dispersion degree was only 42.52%. After standing in slickwater with a mass concentration of 0.1% for 2 h, most of the fibers still floated to the upper part of the solution, and the lower part of the system showed a large layer of stratification. The fiber dispersion only increased to 65.75%. The dispersion stability of the unmodified fibers in water and slickwater is poor.

The dispersion of the developed strong-polar fiber in clear water and slick water is shown in Figure 7b. The dispersion time of the strong-polar fiber is 10 s, which can be quickly dispersed, and the fiber is flocculently distributed in the solution. The density of the strong-polarity fiber was slightly higher than that of water. The fibers were mainly distributed in the lower part of the solution after standing for 2 h, and a small section of clear water stratification appeared in the upper part of the system. The fibers were not stratified at all in water with a 100% dispersion degree. After standing in slickwater with a mass fraction of 0.1% for 2 h, the fibers still achieved rapid, uniform, and stable dispersion. The dispersion behavior was excellent.

This is due to the fact that after the fibers have been modified by two key improvement processes, the introduction of strong-polar groups and surface grafting, the fibers have stronger hydrophilicity. The density of the fiber materials is close to the density of the solution. The dispersion stability in the solution has been greatly improved. The two improvement processes are indispensable. The strong-polarity fibers obtained by this method can better satisfy the requirements of the rapid and uniform dispersion of fiber for fiber-accompanied injection fracturing.

4.3. Evaluation of Fiber's Static Suspension Performance

When fibers are added to the slickwater, the fibers disperse in the fracturing fluid to form a fiber-based network, which prevents the proppant from settling and thus improves the proppant carrying capacity of the system. The settling and placement of proppants in different concentrations of unmodified fiber–slickwater and strong-polarity fiber–slickwater are shown in Figure 8. The corresponding parameters are listed in Table 2.

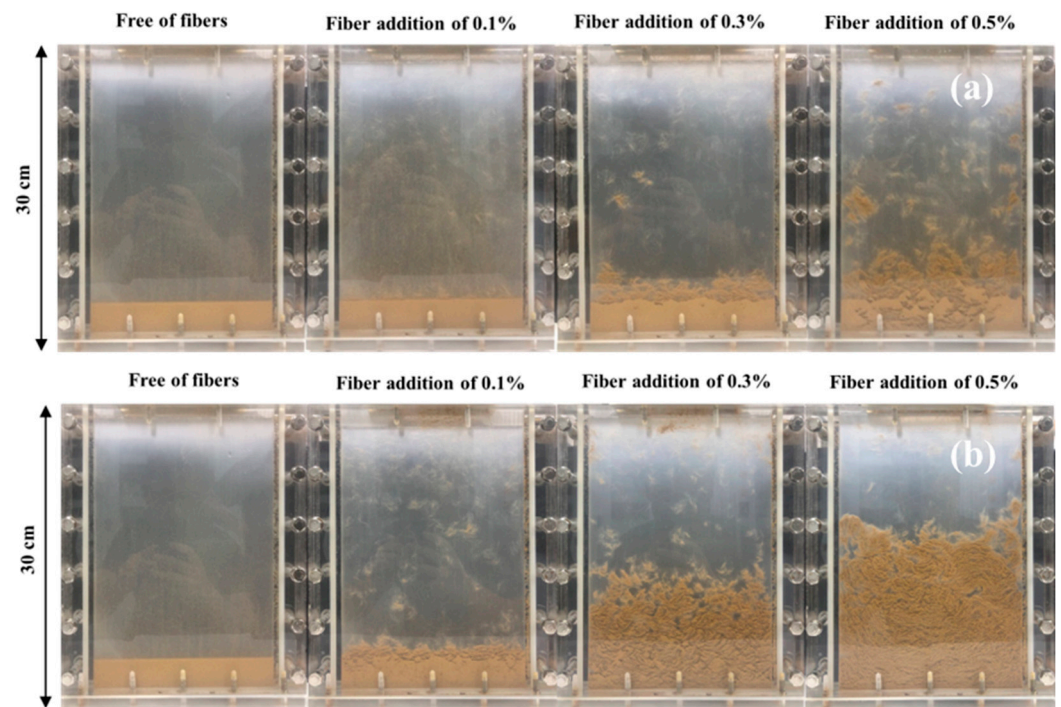


Figure 8. Static settling results of proppants in unmodified fiber-slickwater and strong-polarity fiber-slickwater with different concentrations. (a) unmodified-fiber-slickwater. (b) strong-polarity-fiber-slickwater.

Table 2. Static settling parameters of proppants in slickwater with different fibers.

Fibers	Concentration of Fibers	Settling Time of Proppant/s	The Laying Height of the Proppant/cm
/	0.00%	45	4.7
Unmodified fiber	0.10%	102	4.7
Unmodified fiber	0.30%	160	6.2
Unmodified fiber	0.50%	232	8.7
Strong-polarity fiber	0.10%	129	5.8
Strong-polarity fiber	0.30%	195	14.2
Strong-polarity fiber	0.50%	283	19.1

After adding the fiber materials to the slickwater, the fibers form a floc structure in the system. The addition of fibers can change the settlement behavior of proppants in the fracturing fluid, and the proppant settlement no longer obeys Stokes' law. The interaction between the fibers and proppants prevents the proppants from settling, thereby improving the proppant-carrying capacity of the system. With the gradual increase in suspended proppants, the flocculent fibers and proppant settle synchronously. This composite structure is gradually compacted during the settlement process and eventually becomes a part of the proppant pack. The rest of the flocculent fiber-proppant mixture is suspended in the system, which is beneficial for sufficient proppant placement in the whole artificial fracture.

As shown in Figure 8a and Table 2, in the slickwater without adding any fibers, the proppants settle rapidly in the system and can completely settle after 45 s. The height of the sand bank is low, only 4.7 cm. When 0.1% unmodified fibers were added to the slickwater, the settling velocity of the proppants was significantly reduced. The settling time was increased to 102 s, but the height of the sand bank was basically unchanged (4.7 cm). With a continuous increase of fiber amount, both the settling time and the height of proppant bank increase. When the mass fraction of the fibers reached 0.5%, the fiber-coated proppants formed a heterogeneous and loose cluster-like sand bank distribution. The proppant settlement time reached 232 s, which was 4.1 times higher than that of

the non-fiber system. The proppant bank height was 8.7 cm, which was 85.1% higher than that of the non-fiber system.

As shown in Figure 8b and Table 2, the settling time of proppants was increased to 129 s in the slickwater system with 0.1% mass concentration of strong-polarity fibers. The settling time was 26.5% higher than that of the unmodified-fiber system with the same concentration. The proppant bank height was 5.8 cm, which was 23.4% higher than that of the unmodified-fiber system. With a continuous increase in the fiber amount, both the settling time and the height of proppant bank increase markedly. When the mass fraction of the fibers reached 0.5%, the fiber-coated proppants formed a uniform and dense cluster-like sand bank distribution. The settling time was increased to 283 s, which was 22.0% higher than that of the unmodified-fiber system with the same concentration. The proppant bank height was 19.1 cm, which was about 119.5% higher than that of the unmodified-fiber system. Compared with unmodified fibers, strong-polarity fiber materials can achieve higher proppant suspension capacity and better placement results at a lower dosage, showing the obvious advantages of strong-polarity fibers.

4.4. Evaluation of Dynamic Proppant-Carrying Capacity of Fibers

The experiment of proppant transport in the fiber–slickwater system was carried out using the plate fracture visualization device. The impact of adding strong-polarity fibers on the proppant transport and the proppant bank morphology was investigated. The results are shown in Figure 9. The placement of 40/70 mesh quartz sand in slickwater and fiber–slickwater is shown in Figure 9a and b, respectively.

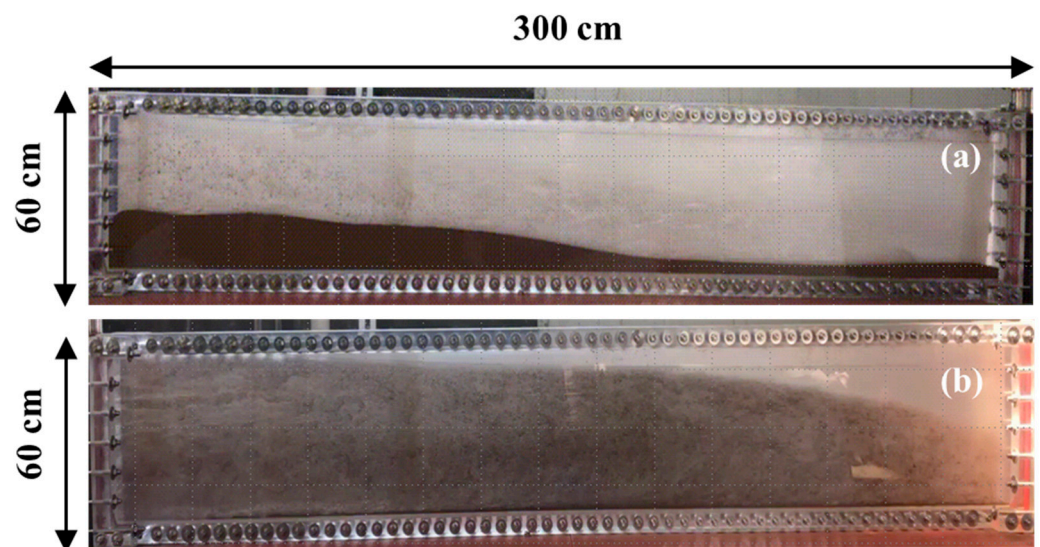


Figure 9. Placement of 40/70 mesh quartz sand. (a) Slickwater without fibers. (b) Slickwater with 0.4% strong-polarity fibers.

Figure 9a shows the resulting proppant bank with 40/70 mesh proppants in slickwater without fibers. Due to the weak proppant-carrying capacity of single slickwater, the proppant particles continue to settle from the fluid to the bottom of the fracture under the action of gravity. The proppants settled more at the fracture inlet and then were pushed to the tip of the fracture to form a sand bank. The further injection of proppants increased the length and height of the sand bank. The height growth process of the whole sand bank was slow. The equilibrium height was not reached after over 50 min.

Figure 9b shows the resulting proppant bank with 40/70 mesh proppants in slickwater containing 0.4% strong-polarity fibers. Other conditions are the same as those of Figure 8. In the slickwater fracturing fluid with strong-polarity fibers, the fibers were wound to form clusters, which can suspend and drag the proppants and carry the proppants into the fracture tip, improving the supporting efficiency at the inner fracture. By using the

fluid with 0.4 mass fraction of strong-polarity fibers, the proppant transport distance can be increased by more than 50%. The growth of the sand bank is faster, and the height of the proppant bank is higher during the same accumulation time. The proppant bank consists of a large number of uncompacted fiber–proppant masses. At the same time, the proppant placement profile is greatly improved, making the sand bank more uniform.

4.5. Evaluation of Proppant Backflow Prevention Performance of Fibers

The variation of the critical sand flow-out rate of the proppant pack was tested at different closing pressure conditions. This parameter was used to characterize the proppant backflow prevention ability of the strong-polarity fibers. The impacts of 0.5% mass-fraction strong-polarity fibers and unmodified fibers on the critical sand flow-out rate of the 40/70 mesh proppant pack are shown in Figure 10. As can be seen from Figure 10, the closing pressure has a great influence on the critical sand flow-out rate of the proppant bank. Under the 2 MPa closure pressure condition, the critical sand flow-out rate of the proppant bank generated using 0.5% mass-fraction unmodified fibers was 117 mL/min. Under the same condition, the critical sand flow-out rate of that generated using strong-polarity fibers was 246 mL/min. With the increase in the closure pressure, the critical sand flow-out rate of the two proppant banks increased rapidly. Under the closure pressure of 8 MPa, the critical sand flow-out rate of the proppant bank generated using 0.5% mass-fraction unmodified fibers was 341 mL/min. Under the same condition, the critical sand flow-out rate of that generated using strong-polarity fibers was 723 mL/min. Under the tested closure pressure ranging from 2–10 MPa, the critical sand flow-out rate of the proppant bank can be increased by more than one time by adding strong-polarity fibers compared with using unmodified fibers.

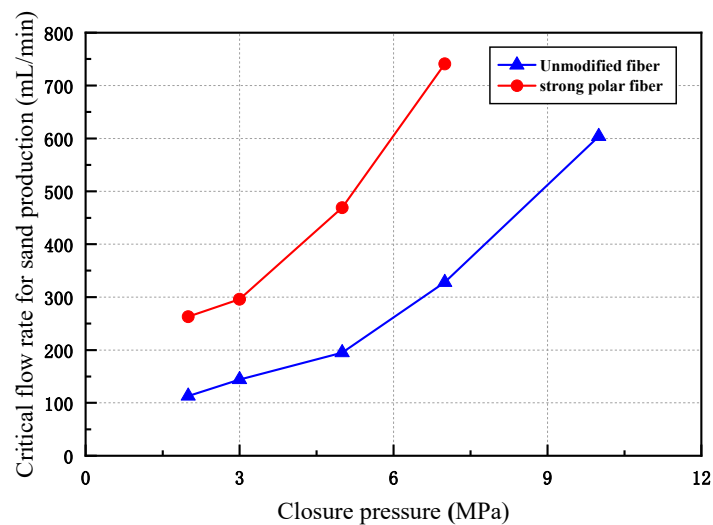


Figure 10. Impacts of different fiber materials on the critical sand flow-out rate of 40/70 mesh proppant pack.

The placement results of the two types of proppants with different fibers within the artificial fractures after flooding are shown in Figure 11. The proppant pack formed by adding 0.5% mass-fraction unmodified fibers shows that the proppant particles were eroded by the fluid, and the proppant profile at the inlet section was missing after flooding. At the same mass fraction, the proppant pack generated using the strong-polarity fibers exhibits better structural strength and is more stable. After the flooding test, the proppant profile can still be kept uniform and complete. There is no obvious missing part in the proppant pack. The post-flooding proppant profile of the sand pack intuitively indicates the outstanding advantages of the strong-polarity fiber material developed in this paper in preventing proppant backflow. It can better improve the stability of the proppant bank and effectively solve the sand production problem in the post-fracturing production process.



Figure 11. Proppant particle distribution after flooding of the proppant pack. (The red circle represents the missing part of the proppant pack after the experiment.).

5. Conclusions

In this paper, a new type of strong-polarity fiber was developed for the purpose of preventing proppant back production. Through the introduction of strong-polarity functional monomers and surface modification, the coupling effect between fibers and proppant particles was strengthened, improving the stability of the fiber and proppant composite structure and the ability of preventing proppant backflow. Experiments were performed to analyze the functional characteristics and backflow mitigation mechanisms. The following conclusions can be drawn:

- (1) The proppant particles injected into the fracture are affected by the drag force of the fluid. When the backflow force is greater than the backflow resistance, the proppant particles transition from a stable state to an unstable one and were carried into the wellbore by the fluid, resulting in proppant backflow. Adding fibers can enhance the cohesion of the proppants, improve the stability of the proppant pack, greatly increase the critical sand flow-out rate, and achieve the purpose of preventing and controlling the backflow of proppant.
- (2) By introducing strong-polarity functional monomers and surface grafting modifications, the hydrophilic properties and material density of the modified fibers were improved, and the coupling between fibers and proppant particles was enhanced. Meanwhile, the density of the material is also close to the density of the solution. Thus, the dispersion performance of the developed strong-polarity fibers is excellent. The fibers can be quickly dispersed in less than 10 s, and 100% dispersion can be achieved in clean water and slickwater, which is significantly better than that of unmodified fibers.
- (3) Adding the strong-polarity fibers significantly improves the proppant suspension ability of slickwater-based fracturing fluid. The filament winding forms a flocculent structure that plays a key role in the suspension and dragging of the proppants, which can effectively reduce the settling velocity of proppants in the fracture. The strong-polarity fibers with a 0.4% mass fraction can increase the proppant transport distance by more than 50%, improve the supporting effect of proppants in the inner fracture, and greatly enhance the proppant accumulation volume. The proppant placement profile can be improved, and the placement becomes more uniform.
- (4) Compared to unmodified fibers, strong-polarity fiber materials can effectively solve the sand production problem during the production process of fractured wells. By

using strong-polarity fiber materials, the coupling effect between fibers and proppant particles is improved, and the cohesive force inside the proppant sand is enhanced. Within the closed pressure range of 2–10 MPa, the critical sand flow-out rate of the proppant bank can be increased by more than twice. After flooding, the proppant can still be uniformly laid in artificial cracks, greatly enhancing the stability of the proppant pack.

Author Contributions: Conceptualization, Y.M.; Methodology, P.C., K.W. and S.W.; Investigation, Y.X., S.W., Q.M. and M.L.; Data curation, M.L.; Writing—original draft, Y.X., P.C., K.W., Y.M. and J.Z.; Writing—review & editing, Q.M. and J.Z. All authors have read and agreed to the published version of the manuscript.

Funding: This research received no external funding.

Data Availability Statement: The data presented in this study are available on request from the corresponding author.

Conflicts of Interest: Authors Yang Xu, Ping Chen, Kun Wang, Suoliang Wang, Qingcong Meng and Mingqi Li were employed by the Research Institute of Drilling & Production Engineering, CNPC Chuanqing Drilling Engineering Company Limited. The remaining authors declare that the research was conducted in the absence of any commercial or financial relationships that could be construed as a potential conflict of interest.

References

- Jie, Y.; Yang, J.; Zhou, D.; Wang, H.; Zou, Y.; Liu, Y.; Zhang, Y. Study on the Optimal Volume Fracturing Design for Horizontal Wells in Tight Oil Reservoirs. *Sustainability* **2022**, *14*, 15531. [[CrossRef](#)]
- Xu, J.; Liu, R.; Liu, H. Optimization of shut-in time based on saturation rebalancing in volume-fractured tight oil reservoirs. *Pet. Explor. Dev.* **2023**, *50*, 1445–1454. [[CrossRef](#)]
- Zeng, Q.; Bo, L.; Liu, L.; Li, X.; Sun, J.; Huang, Z.; Yao, J. Analysis of fracture propagation and shale gas production by intensive volume fracturing. *Appl. Math. Mech.* **2023**, *44*, 1385–1408. [[CrossRef](#)]
- Wen, Y.; Liu, L.; Huang, Y.; Liu, H.; Sui, M. Cause Analysis and Preventive Measures for Sand Production in Gas Wells of Sulige Gas Field. *ACS Omega* **2023**, *8*, 30590–30597. [[CrossRef](#)] [[PubMed](#)]
- Zhang, T.; Tang, T.; Guo, J.; Zhou, H.; Liu, Y.; Zhang, Y.; Zeng, X. Experimental study on proppant-carrying migration and settlement of slickwater in narrow plate fractures based on PIV/PTV. *Petroleum* **2023**, *in press*. [[CrossRef](#)]
- Nguyen, P.D.; Weaver, J.D.; Rickman, R.D.; Sanders, M.W. Remediation of Proppant Flowback—Laboratory and Field Studies. In Proceedings of the European Formation Damage Conference, Scheveningen, The Netherlands, 30 May–1 June 2007; p. 106108. [[CrossRef](#)]
- Canon, J.M.; Romero, D.J.; Pham, T.T.; Valko, P.P. Avoiding Proppant Flowback in Tight-Gas Completions with Improved Fracture Design. In Proceedings of the SPE Annual Technical Conference and Exhibition, Denver, CO, USA, 5–8 October 2003; p. 84310. [[CrossRef](#)]
- Zhang, H.; Yang, S.; Liu, D.; Li, Y.; Luo, W.; Li, J. Wellbore cleaning technologies for shale-gas horizontal wells: Difficulties and countermeasures. *Nat. Gas Ind. B* **2020**, *7*, 190–195. [[CrossRef](#)]
- Wee, S.K.; Yap, Y.J. CFD study of sand erosion in pipeline. *J. Pet. Sci. Eng.* **2019**, *176*, 269–278. [[CrossRef](#)]
- Li, B.L. *Study on Multiple Temporal and Spatial Scale Flow Mechanism in Stimulated Tight Reservoir*; China University of Petroleum (East China): Qingdao, China, 2020.
- Yan, G.; Li, Z.; Torres, S.A.G.; Scheuermann, A.; Li, L. Transient Two-Phase Flow in Porous Media: A Literature Review and Engineering Application in Geotechnics. *Geotechnics* **2022**, *2*, 32–90. [[CrossRef](#)]
- Liu, X.J. *Research on the Law of Proppant Migration In hydraulic Fracturing Fractures*; China University of Petroleum (Beijing): Beijing, China, 2021. [[CrossRef](#)]
- Chen, Y.; Sang, Y.; Guo, J.; Yang, J.; Chen, W.; Tang, B.; Feng, F.; Gou, X.; Zhang, Y. Experimental Study on the Backflow Mechanism of Proppants in Induced Fractures and Fiber Sand Control Under the Condition of Large-Scale and Fully Measurable Flow Field. *ACS Omega* **2023**, *8*, 42467–42478. [[CrossRef](#)]
- Salahi, A.; Dehghan, A.N.; Sheikhzakariaee, S.J.; Davarpanah, A. Sand production control mechanisms during oil well production and construction. *Pet. Res.* **2021**, *6*, 361–367. [[CrossRef](#)]
- Yang, X.; Wu, T.; Ren, L.; Huang, S.; Wang, S.; Li, J.; Liu, J.; Zhang, J.; Chen, F.; Chen, H. Mechanisms of Stress Sensitivity on Artificial Fracture Conductivity in the Flowback Stage of Shale Gas Wells. *Processes* **2023**, *11*, 2760. [[CrossRef](#)]
- McLennan, J.; Walton, I.; Moore, J.; Brinton, D.; Lund, J. Proppant backflow: Mechanical and flow considerations. *Geothermics* **2015**, *57*, 224–237. [[CrossRef](#)]

17. Zhou, F.; Zong, Y.; Liu, Y.; Yang, X.; Xiong, C.; Zhang, S.; Sun, L.; Wang, J.; Li, J.; Guang, Z. Application and Study of Fine-Silty Sand Control Technique Using Fiber-Complex High-Pressure Pack in Sebei Gas Reservoir. In Proceedings of the SPE International Symposium and Exhibition on Formation Damage Control, Lafayette, LA, USA, 15–17 February 2006; p. 97832. [CrossRef]
18. Al-Ghurairi, F.; Solares, R.; Bartko, K.; Sierra, L. Results From a Field Trial Using New Additives for Fracture Conductivity Enhancement in a High-Gas Screenless Completion in the Jauf Reservoir, Saudi Arabia. In Proceedings of the SPE International Symposium and Exhibition on Formation Damage Control, Lafayette, LA, USA, 15–17 February 2006; p. 98088. [CrossRef]
19. Zhu, K.; Guo, D.; Zeng, X.; Li, S.; Liu, C. Proppant flowback control in coal bed methane wells: Experimental study and field application. *Int. J. Oil Gas Coal Technol.* **2014**, *7*, 189. [CrossRef]
20. Hu, Y.M.; Zhao, Z.F.; Li, X.W.; Chen, B.C.; Li, Z. Experimental study on proppant reflux resistance of fiber network under high gas injection rate in Yulin gas storage. *Fault-Block Oil Gas Field* **2021**, *28*, 786–791. [CrossRef]
21. Zhao, H.F.; Wang, W.; Jiang, C.Y.; Tian, J.C.; Mu, E.F. Study on fibrous fracturing fluid properties. *Drill. Prod. Technol.* **2017**, *40*, 90–92.
22. Jiang, Q.H.; Yang, X.T.; Yu, X.X.; Liu, J.Q.; Tang, L. Research progresses of slick-water drag reducer at home and abroad. *Chem. Ind. Eng.* **2022**, *39*, 76–83. [CrossRef]
23. Tang, B.T. Optimization of Backflow Parameters for Fractured Shale Gas Wells with Prevention of Proppant Reflow. Master's Thesis, Southwest Petroleum University, Chengdu, China, 2019. [CrossRef]
24. Sun, Z.M.; Lu, X.C.; Jia, X.C.; Bai, Y.S.; Hu, W.X. Optimization of Mercury Intrusion Capillary Pressure Measurement for Characterizing the Pore Structure of Tight Rocks. *J. Nanosci. Nanotechnol.* **2017**, *17*, 6242–6251. [CrossRef]
25. Nguyen, P.D.; Weaver, J.D.; Dewprashad, B.T.; Parker, M.A.; Terracina, J.M. Enhancing Fracture Conductivity Through Surface Modification of Proppant. In Proceedings of the SPE Formation Damage Control Conference, Lafayette, LA, USA, 18–19 February 1998; p. 39428. [CrossRef]
26. Cheng, Y.S. Study on the Mechanism of Proppant Backflow after Fracturing and Its Influence. Master's Thesis, China University of Geosciences (Beijing), Wuhan, China, 2021.
27. Ramones, M.; Rachid, R.; Milne, A.; Pelaez, K.; Gutierrez, L.; Madrid, O.; Ponce, G.; Ponce, O.; Cruz, S. Innovative Fiber-Based Proppant Flowback Control Technique Unlocks Reservoir Potential. In Proceedings of the SPE Latin America and Caribbean Petroleum Engineering Conference, Maracaibo, Venezuela, 21–23 May 2014; p. D011S003R002. [CrossRef]
28. Pitoni, E.; Devia, F.; James, S.G.; Heitmann, N. Screenless Completions: Cost-Effective Sand Control in the Adriatic Sea. *SPE Drill. Complet.* **2000**, *15*, 293–297. [CrossRef]
29. Bedford, A.; Stern, M. Toward A Diffusing Continuum Theory of Composite Materials. *J. Appl. Mech.* **1971**, *38*, 8–14. [CrossRef]
30. Lv, F.M.; Zhou, J.; Song, Q.W.; Zhong, Y. Research on fibrous composite fracturing sand control technique and its application. *Oil Drill. Prod. Technol.* **2008**, *30*, 97–100. [CrossRef]
31. Chen, X.L.; Ding, S.H.; Yuan, X.H. Application of fibre filler fracturing technology in the third region of xinjiang oilfield. *Drill. Prod. Technol.* **2013**, *36*, 61–63.
32. Wu, G.D. Laboratory research on control fracturing proppant backflow with fiber. *Drill. Prod. Technol.* **2012**, *35*, 88–90. [CrossRef]
33. Guo, G.; Xue, X.J.; Fan, H.B.; Liu, J.; Li, K.; Wu, J. Development and application of fiber slick water fracturing fluid for dense reservoirs. *Fault-Block Oil Gas Field* **2019**, *26*, 269–272. [CrossRef]
34. Yang, G.W.; Bai, J.W.; Chi, X.M.; Luo, M.L.; Yi, D.Q.; Xue, Y.F.; Zhang, J.F. Study on performance and surface modification of the degradable fiber plugging agent hydraulic fracturing. *Appl. Chem. Ind.* **2014**, *43*, 1431–1434. [CrossRef]
35. Song, B.; Bismarck, A.; Tahhan, R.; Springer, J. A Generalized Drop Length–Height Method for Determination of Contact Angle in Drop-on-Fiber Systems. *J. Colloid Interface Sci.* **1998**, *197*, 68–77. [CrossRef]
36. SY/T 5185-2016; Performance Evaluation Method of Gravel Packing Sand Control Water-Based Sand-Carrying Fluid. China National Energy Administration: Beijing, China, 2016. Available online: <https://d.wanfangdata.com.cn/standard/SY/T%205185-2016> (accessed on 2 March 2024).

Disclaimer/Publisher's Note: The statements, opinions and data contained in all publications are solely those of the individual author(s) and contributor(s) and not of MDPI and/or the editor(s). MDPI and/or the editor(s) disclaim responsibility for any injury to people or property resulting from any ideas, methods, instructions or products referred to in the content.